ISSN 1023-1935, Russian Journal of Electrochemistry, 2017, Vol. 53, No. 2, pp. 140–146. © Pleiades Publishing, Ltd., 2017.
Published in Russian in Elektrokhimiya, 2017, Vol. 53, No. 2, pp. 157–164.

Electrodeposition and Characterization of Red Selenium Thin Film—Effect of the Substrate on the Nucleation Mechanism[1]

Oualid Dilmi* and Mohamed Benaicha

Energetic and Solid State Electrochemistry Laboratory, Ferhat Abbas-Setif1 University, Setif 19000, Algeria

**e-mail: dilmi_oualid@yahoo.fr*

Received October 16, 2015

Abstract—In this work, cyclic voltammetry (CV) and chronoamperometry (CA) were used to study the electrodeposition mechanism of red selenium on platinum and (ITO) substrates from aqueous solution containing (SeO_2) and sodium citrate as support electrolyte with pH 4.3 at ambient temperature. The potentiostatic current transients were analyzed according to Scharifker–Hills model. The morphological characterization of the deposit was carried out by Scanning Electron Microscopy (SEM), whereas the optical one was realized by UV-Visible spectroscopy. The results shown that the nucleation mechanism of Se on each substrate is instantaneous with a three-dimensional growth of the hemispherical nuclei. The nucleation density (N_0) is exponentially increased with the applied overpotential. Se thin film has an energy gap of about 2.4 eV.

Keywords: electrodeposition, nucleation, selenium, energy gap

DOI: 10.1134/S1023193517020045

1. INTRODUCTION

Owing to its good semiconducting, optical, thermal, electric and piezoelectric properties [1–3], selenium has various physical, chemical, and biological applications in our life [4–7], one of them in particular is the use in solar cells as photoactive thin film [8, 9]. It appears in different phases. The amorphous phase (red, brown and black) exhibits low electronic conductivity. The crystalline phases, include several solid allotropes, namely, the rhombohedral one, the α, β and γ monoclinic ones and the trigonal (hexagonal) one. Hexagonal Se is gray and it is the densest and the most stable of all phases [10]. Nowadays, various methods are used to obtain selenium and its alloys films such as sol–gel [11, 12], hydrothermal [13–15], spray pyrolysis [16, 17], template method [18, 19], chemical vapor deposition [20, 21] and electrodeposition methods [22–25]. The electrodeposition of thin films is considered as one of the most promising ways due to the ability to control the thickness, a large-area deposition, a simple process, good adhesion, reproducibility and a low manufacturing process cost [9]. Several studies have used the electrodeposition method to make electrodeposited selenium, these studies focus mainly on the morphology of the deposits and their qualities [8, 22, 25–27] but are not interested to study the formation mechanism of the selenium deposit and the influences of the substrate on this mechanism, for this reason our study is devoted on the determination of the nucleation and growth mechanism of the germs during the electrodeposition of selenium film on different substrates. The goal of this work is to study the electrodeposition mechanism of the red selenium on substrates (platinum and ITO) in acid medium (pH 4.3) at ambient temperature starting from an aqueous solution based on selenium dioxide SeO_2 in the presence of sodium citrate as support electrolyte by a model based on Scharifker–Hills calculations which established to determine the nucleation and growth mechanism [28, 29]. The nucleation density and the energy gap were also investigated.

2. EXPERIMENTAL

Red selenium dioxide SeO_2 (Sigma-Aldrich, 99.99%) and sodium citrate tribasic dihydrate $C_6H_5Na_3O_7 \cdot 2H_2O$ (Fluka, 99%) powders used to prepare our electrodeposition bath. Stationary electrochemical measurements (cyclic voltammetry (CV) and chronoamperometry (CA)) were carried out using a system Voltalab PGZ 301 controlled by a computer (software Volta-Master4) with a cell of three electrodes; the saturated calomel electrode (SCE) as reference electrode, the platinum wire as counter electrode, the work electrode was used as platinum and ITO (Indium Tin Oxide). The platinum substrate was cleaned in the nitric acid during 30 s, whereas the ITO substrate was first cleaned in acetone for five minutes, then in ethanol for

[1] The article is published in the original.

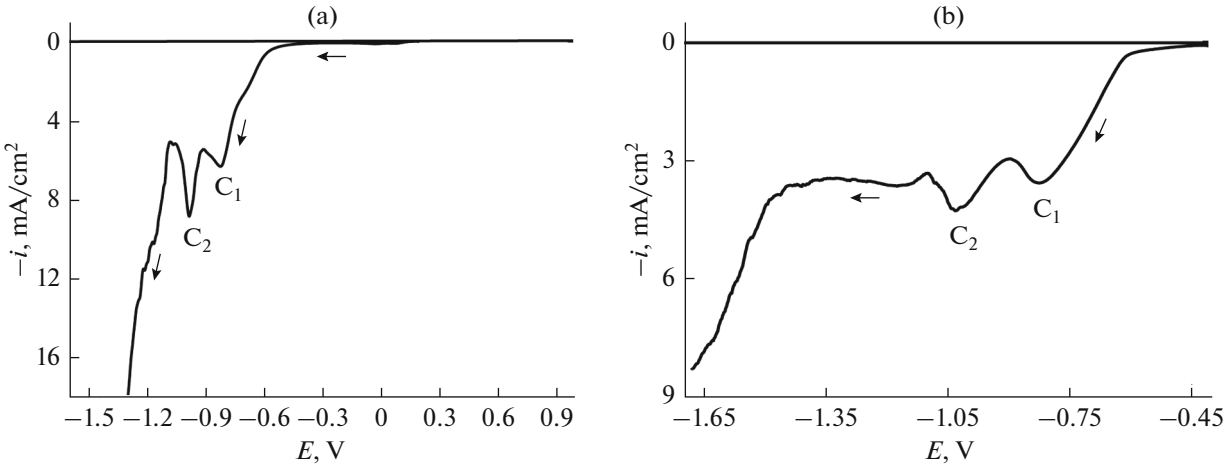

Fig. 1. Voltammograms of SeO_2 aqueous solution (50 mM) in medium of sodium citrate (0.15 M) (pH 4.3) on (a) platinum and (b) ITO electrodes with scanning rate $v = 5$ mV s^{-1}.

10 min, in the nitric acid (30%) during two minutes and finally well rinsed with distilled water.

In this study, we used for all handling an aqueous solution of (50 mM) selenium dioxide SeO_2 (which dissolves in water and gives ($HSeO_3^-$)) and (0.15 M) sodium citrate. The pH 4.3 was fixed by addition of some drops of hydrochloric acid (HC1). For each substrate, cyclic voltammogram has been traced to determine the electrodeposition potentials of selenium, after that these potentials were applied in chronoamperometry method. The surface morphology of electrodeposited selenium film on ITO substrate was investigated using a JSM-7001F (SEM). The UV-Visible transmittance spectra have been recorded with a Shimadzu UV-1800 UV-Visible scanning spectrophotometer.

3. RESULTS AND DISCUSSION

The voltammetry was performed in order to identify the presence of electrodeposition processes and to verify the electrochemical behavior of electrodes in the electrodeposition bath. Figure 1 represents linear voltammograms of the cathodic part for our solution traced on platinum (a) and ITO (b) electrodes with a scanning rate of $v = 5$ mV s^{-1}. We can observe from the curve (a), during cathodic scan from the abandonment potential, two cathodic peaks (C_1 at −0.82 V and C_2 at −0.97 V vs. SCE) relating respectively to formation of elemental Se, and release of H_2Se gas [30, 31].

In curve (b), we observe also two cathodic peaks (C_1 and C_2). The peak C1 locates at −0.82 V vs. SCE relates to formation of selenium thin film on the electrode surface, the peak C_2 locates at −1.02 V vs. SCE corresponds to release of H_2Se gas [9]. In other part the irreversible electroreduction of the tin oxide can also take place [32].

Scharifker and Hills have developed theoretical models to describe the nucleation process during the initial few seconds of electrodeposition using chronoamperometric curves. According to the three-dimensional (3D) nucleation model, two limiting cases referring to instantaneous and progressive nucleation modes have been considered. Instantaneous nucleation corresponds to fast growth of nuclei on many active sites, all activated during the electroreduction step, whereas, progressive nucleation describe a slower growth of nuclei on a small number of active sites, all activated at the same time [28, 29].

In order to determine the nucleation and growth mechanism of the selenium deposited on each substrate, chronoamperograms corresponding to electrodeposition potentials has been recorded. Figure 2 represents the variation of the current density (i) according to the time (t) traced for the two substrates with different imposted potentials. We observe an abrupt decreases in absolute value of the current density at the beginning which is related to double layer charging and the necessary time for the formation of the first germs on the active sites of the electrode surface, after that the current density increases gradually until a maximum value (i_m) corresponds a maximum time (t_m) follows to the growth of the germs which results to the boost of active sites number in the surface of the electrode, in the last step the current reduces and tends towards a constant value (limit current), that leads to a diffusion mode which limits the process [33, 34]. It's clear that the i_m increases with increasing the imposed potential but t_m decrease; this shows that the acceleration of electrocrystallization phenomena is more favored while the imposed potential is sufficiently cathodic. This is a typical response of the current transients for a nucleation and growth three dimensional (3D) under diffusional control [28, 35].

It's possible to analyze the first stages of electrodeposition to determine the corresponding nucleation

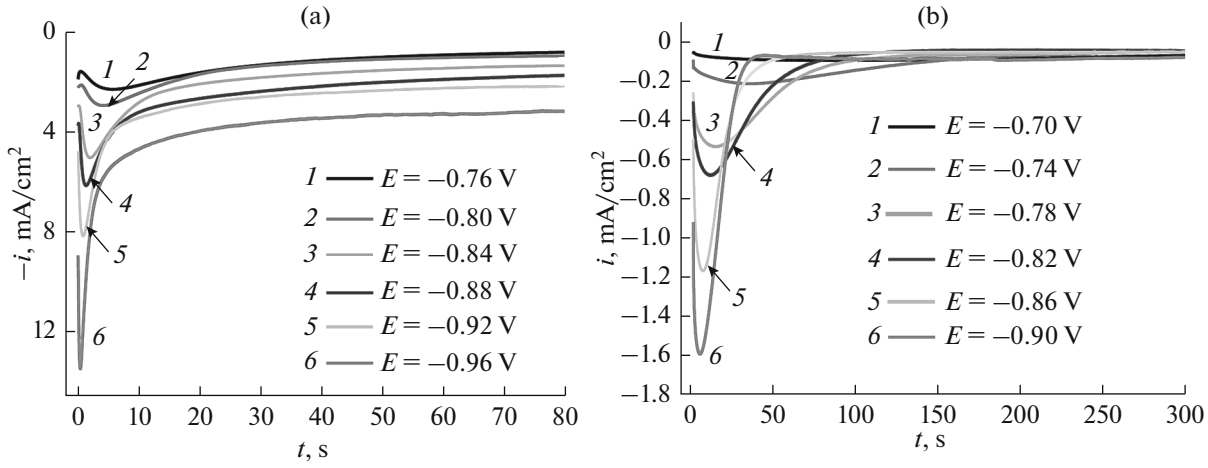

Fig. 2. Current transients for selenium electrodeposition on (a) platinum and (b) ITO electrodes at different applied potentials.

mechanism using the first parts of the chronoamperograms i.e. before the diffusion step limit established, in this case, from Scharifker–Hills model, there is a linear variation of the current density (i) with $t^{1/2}$ (i vs. ($t^{1/2}$) is a straight line) for instantaneous nucleation and a linear variation of i vs. ($t^{3/2}$) for progressive nucleation according to equations (1) and (2) [28, 29].

$$i = zFD^{3/2}C^{1/2}N_0Kt^{1/2}, \quad K = \left(\frac{8\pi CM}{\rho}\right)^{1/2}, \qquad (1)$$

$$i = zFD^{3/2}C^{1/2}AN_0K't^{3/2}, \quad K' = \frac{4}{3}\left(\frac{8\pi CM}{\rho}\right)^{1/2}, \qquad (2)$$

where zF is the molar charge of electrodepositing species, D is the diffusion coefficient, C the bulk concentration of the electroactive species, N_0 the nucleation density (i.e. the number of active sites per area unit), t is the time, M is the atomic weight and ρ is the density of the deposit. Figure 3 shows the curves i vs. ($t^{1/2}$) and i vs. ($t^{3/2}$) from the first stages of the chronoamperograms obtained previously where we observe an ideal linearity for the curves i vs. ($t^{1/2}$) and nonlinearity for the curves i vs. ($t^{3/2}$) which shows that the selenium electrodeposition on these substrates follows the instantaneous nucleation type.

The non-dimensional plots of $(i/i_m)^2$ vs. (t/t_m) are usually used to distinguish between instantaneous and progressive nucleation processes, by comparing theoretical and experimental curves. To confirm the nucleation type and growth we have converted the curves i vs. t into adimensional form according to Scharifker–Hills model as shown the two equations (3) and (4) [28, 29].

For instantaneous nucleation followed by three-dimensional diffusion-limited growth we have:

$$\left(\frac{i}{i_m}\right)^2 = 1.9542\left(\frac{t_m}{t}\right)\left[1-\exp\left(-1.2564\frac{t}{t_m}\right)\right]^2. \qquad (3)$$

And for progressive nucleation followed by three-dimensional diffusion-limited growth:

$$\left(\frac{i}{i_m}\right)^2 = 1.2254\left(\frac{t_m}{t}\right)\left[1-\exp\left(-2.3367\frac{t^2}{t_m^2}\right)\right]^2. \qquad (4)$$

Figure 4 presents the curves $(i/i_m)^2$ vs. (t/t_m) correspond to the preceding chronoamperograms traced with the theoretical curves correspond to equations (3) and (4) for instantaneous (full line) and progressive (dotted line) nucleation, it's clear that selenium adopts an instantaneous nucleation on the platinum substrate as per Fig. 4a (the experimental curves completely follow the theoretical curve describe the instantaneous nucleation with an except of very small divergence starting from the value $t/t_m > 2.5$), this divergence was explained by several auteurs and reported to the parasitic reaction of hydrogen [36, 37]. For the Fig. 4b we observe a significant divergence compared with the theoretical curve of instantaneous nucleation; may reflect the hydrogen reaction on the surface of the working electrode which influences directly on the number of nucleation sites. Generally selenium adopts also instantaneous nucleation on the ITO substrate (Figs. 3b and 4b).

After the determination of the electrocrystallization mechanism, we can also determine other parameters such as the diffusion coefficient (D) and the nucleation density (N_0) correspond this nucleation model; therefore we have for an instantaneous nucleation:

$$N_0 = 0.065\left(\frac{8\pi CM}{\rho}\right)^{-1/2}\left(\frac{zFC}{i_m t_m}\right)^2, \qquad (5)$$

$$D = \frac{i_m^2 t_m}{0.1629(zFC)^2}, \qquad (6)$$

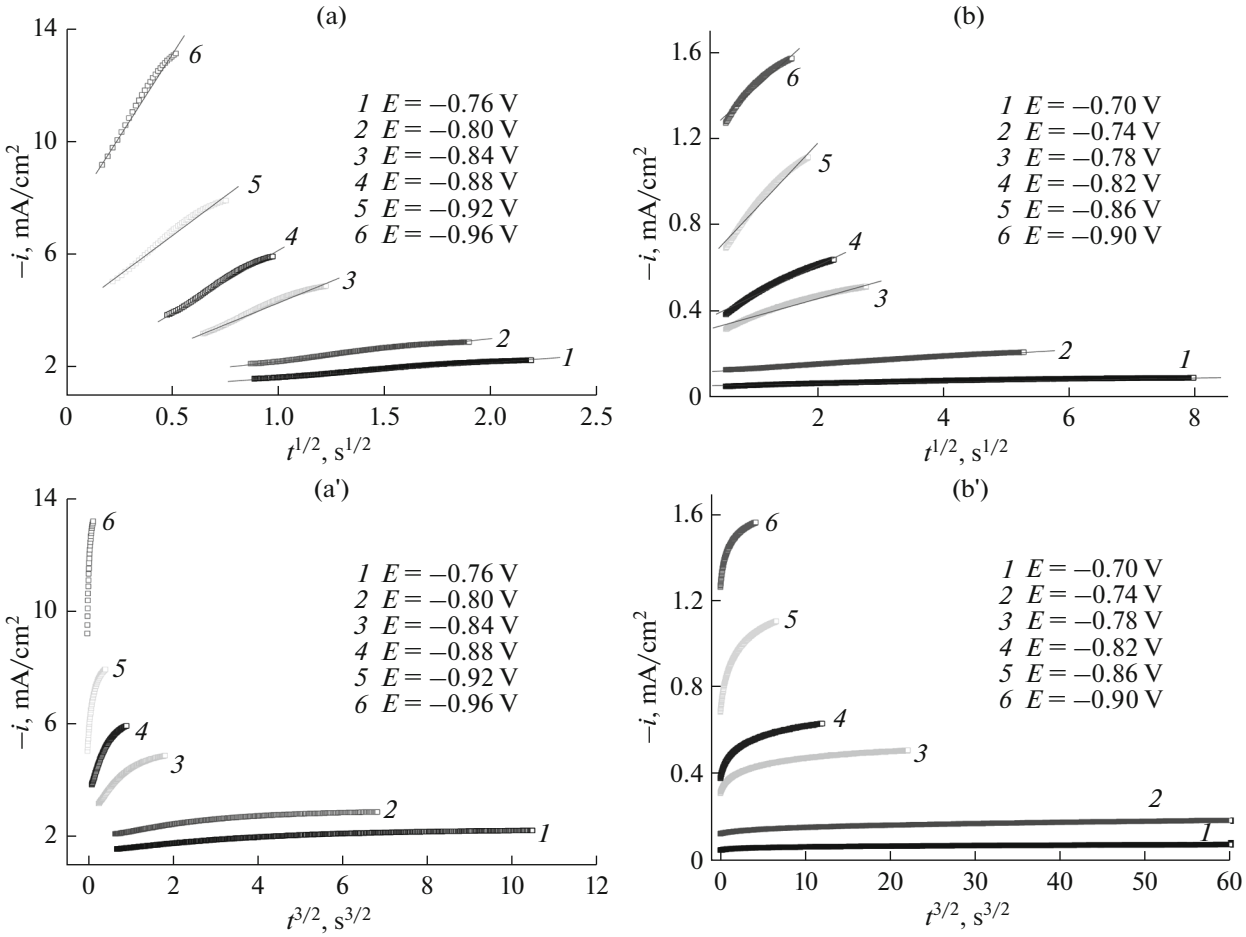

Fig. 3. Dependence of transition current according to $t^{1/2}$ and $t^{3/2}$ for the first stages of nucleation of electrodeposited selenium on (a, a') platinum and (b, b') ITO substrates.

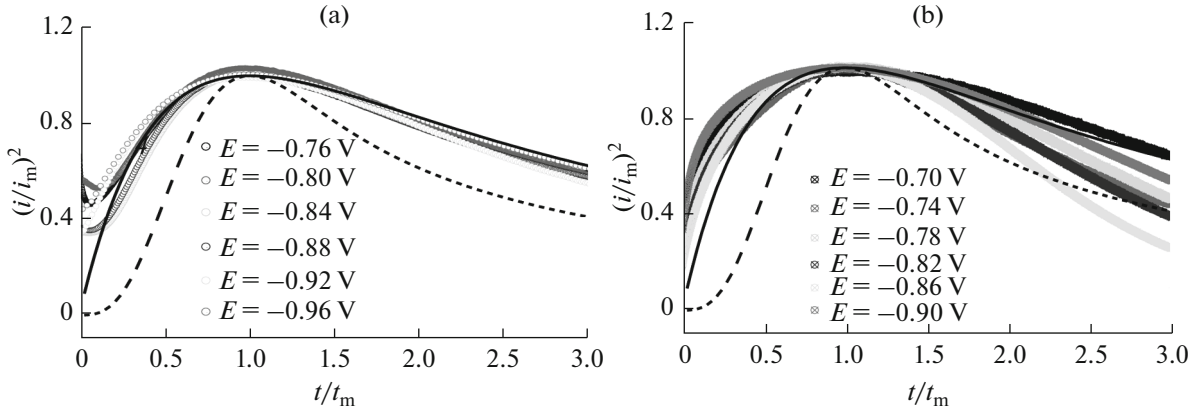

Fig. 4. Dimensionless curves $(i/i_m)^2$ vs. $(t/t_m)^2$ for instantaneous and progressive 3D nucleation from Eqs. (3) and (4) respectively, along with experimental data of selenium electrodeposition on (a) platinum and (b) ITO substrates.

and for a progressive nucleation type:

$$AN_0 = 0.2898\left(\frac{8\pi CM}{\rho}\right)^{-1/2}\frac{(zFC)^2}{i_m^2 t_m^3}, \quad (7)$$

$$D = \frac{i_m^2 t_m}{0.2598(zFC)^2}. \quad (8)$$

Where A is the nucleation rate constant. The values of i_m, t_m and N_0 for the different applied potentials are gathered in the table.

Figure 5 shows the relation between the density of active sites N_0 and the imposed potential E. The N_0 values are quite typical for an instantaneous type of nucleation, which is characterized by a small number

Values of the nucleation density according to the imposed potential

E, V	i_m, mA cm^{-2}	t_m, s	$N_0 \times 10^{-6}$, cm^{-2}
Se/Pt			
−0.76	2.23	5.95	1
−0.80	2.88	4.12	1.13
−0.84	4.96	1.98	1.64
−0.88	6.07	1.31	2.51
−0.92	8.08	0.83	3.52
−0.96	13.37	0.38	6.15
Se/ITO			
−0.70	0.09	82.31	2.9
−0.74	0.21	34.60	3
−0.78	0.53	13.55	3.1
−0.82	0.68	10.19	3.30
−0.86	01.17	05.75	3.50
−0.90	01.59	04.05	3.82

of active sites. In this figure we observe an exponential increase of N_0 with the increase of applied overpotential on the system, This exponential increase is generally understood as the increased activation of more nucleation sites with higher overpotentials, which is consistent with classical nucleation models [38, 39]. Where:

$$N_0 \propto \exp\left(\frac{-e\Delta U}{kT}\right). \quad (9)$$

Figure 6 presents the SEM (Scanning Electron Microscopy) image of electrodeposited selenium on ITO substrate at −0.74 V vs. SCE applied potential for 10 min, the goal of the morphological characterization is to see the morphology of the germs formed on the electrode surface. From this image we observe that the obtained thin layer is very dense with tubular form of grains.

The determination of the transition type direct or indirect, as well as the evaluation of the energy gap for a semiconductor can be carried out by UV-Visible spectrophotometry. A semiconductor absorbs the light at a certain wavelength λ_g which can be related to the gap through the following equation [40]:

$$\lambda_g\ (\text{nm}) = \frac{1240}{E_g}\ (\text{eV}). \quad (10)$$

The extinction of corresponding light follows an exponential law:

$$I = I_0 \exp(-\alpha l). \quad (11)$$

Where l is the penetration length of the light and α is the reverse of the absorption length (the optical absorption coefficient) which is a function with the thickness d, the transmittance T and the reflection coefficient of the semiconductor R, it's given by the following formula [41–44]:

$$\alpha = \frac{1}{d}\ln\left[\frac{(1-R)^2}{2T} + \left(\frac{(1-R)^4}{4T^2} + R^2\right)^{1/2}\right], \quad (12)$$

where the reflection coefficient is given by the following equation:

$$R = \frac{(n_R - 1)^2}{(n_R + 1)^2}, \quad (13)$$

n_R is the refractive index.

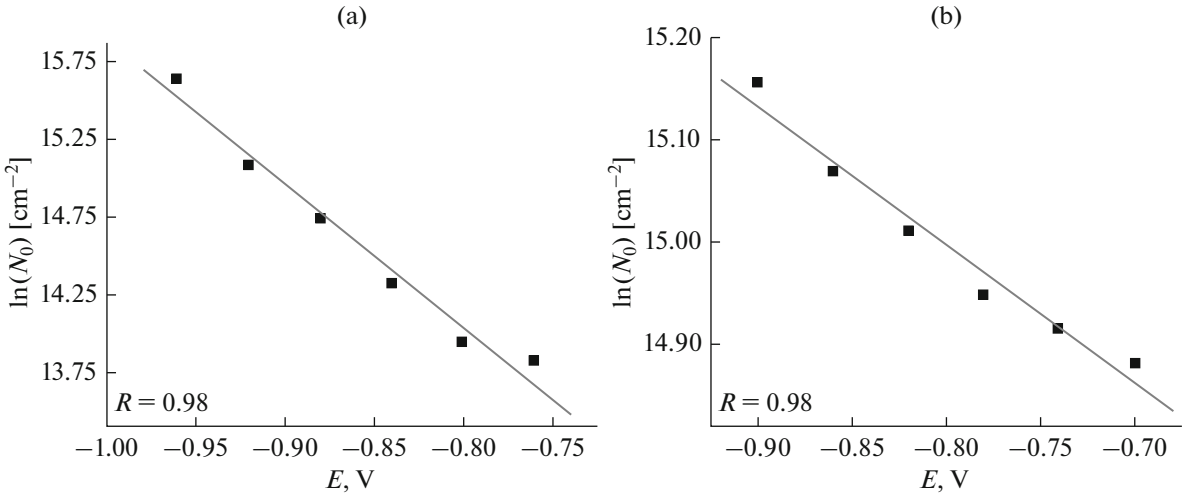

Fig. 5. Dependence of ln(N_0) with E for Se deposited onto (a) Pt and (b) ITO electrodes. Line corresponds to the linear adjustment.

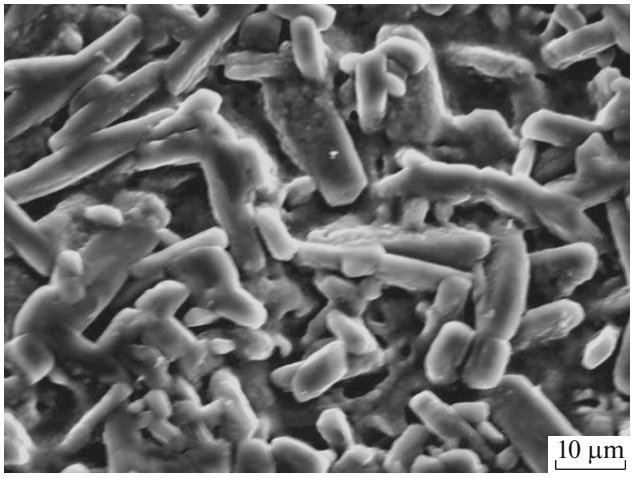

Fig. 6. SEM image of Se deposited on ITO with applied potential –0.74 V vs. SCE during (10 min).

On the other hand the absorption coefficient is a function to the energy of incident photons ($h\nu$) and the energy gap E_g, it's given by the following formula [45]:

$$\alpha h\nu = A\left(h\nu - E_g\right)^n. \quad (14)$$

A is a constant which also depends on the refractive index of the material, the reduced mass and the light speed in the vacuum. The exponent n depends to the transition type: for a direct gap (rutile) $n = 0.5$ and for an indirect gap (anatase) $n = 2$. So it's possible, for each type of particles, to plot the curve:

$$(\alpha h\nu)^{1/n} = f(h\nu). \quad (15)$$

Near the absorption edge, include an affine function. The intersection of the affine part of the curve and the horizontal axis corresponds to the energy gap E_g.

The transmittance spectra UV-Visible for the electrodeposited red selenium (amorphous) on the ITO substrate at –0.74 and –0.86 V vs. SCE potentials, and the plot $(\alpha h\nu)^2$ vs. ($h\nu$) are represented on the Fig. 7; the thicknesses of selenium films obtained at these potentials were estimated using faraday's law as 2.1 and 2.4 μm, respectively. This figure shows that the selenium film is photoactive in the UV-Visible range which translates by the transmission bands at about 435 nm, the plot $(\alpha h\nu)^2$ vs. ($h\nu$) is valid to estimate the gap energy value according to equation (15) ($n = 0.5$ for the red and gray selenium thin layers [46]), from this equation when $\alpha h\nu$ tends towards zero $h\nu$ tends towards E_g, which leads that extrapolation on the axis ($h\nu$) gives us directly the energy gap, in our curve extrapolation gives a value of energy gap for red selenium equal $E_g = 2.4$ eV.

4. CONCLUSIONS

In this study, we present the substrate's influence on the electrodeposition mechanism of red selenium in an acid medium with the sodium citrate (pH 4.3) at ambient temperature using the Scharifker–Hills model. From our research, selenium adopts an instantaneous nucleation 3D under diffusional control on the two substrates: the platinum and the ITO, the nucleation density is exponentially dependent with the imposed potential. From the UV-Visible spectropho-

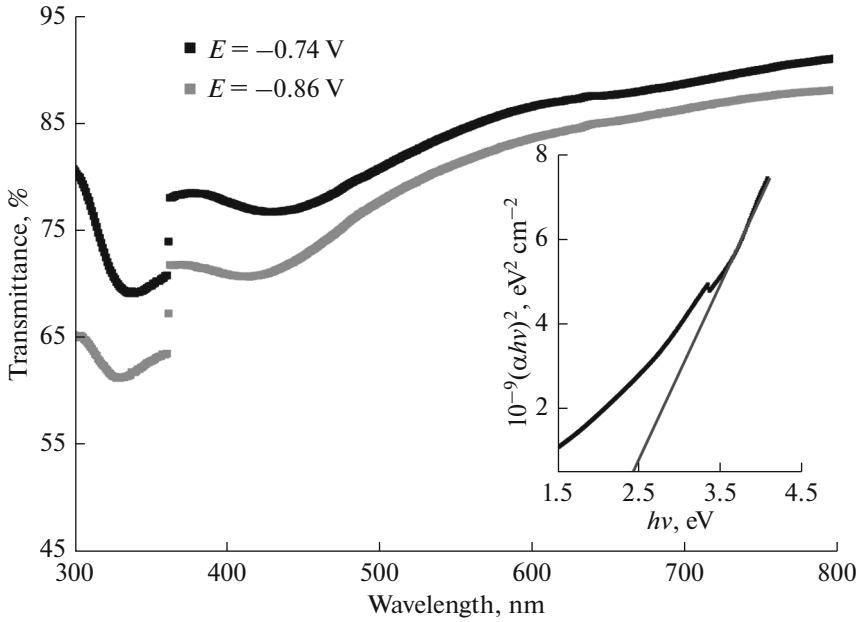

Fig. 7. UV-Visible transmittance spectra for Se electrodeposited film on the ITO during 10 min with the plot $(\alpha h\nu)^2$ vs. ($h\nu$).

tometry of the selenium deposit we found that it's photoactive and has an energy gap of about 2.4 eV.

REFERENCES

1. Randey, R.K., Sahu, S.N., and Chandra, S., *Handbook of Semiconductor Electrodeposition*, N.-Y.: Marcel Dekker Inc., 1996.
2. Johnson, J.A., Saboungi, M.L., Thiyagarajan, P., Scencsits, R., and Meisel, D., *J. Phys. Chem. B*, 1999, vol. 103, p. 59.
3. Gates, B., Mayers, B., Cattle, B., and Xia, Y.N., *Adv. Funct. Mater.*, 2002, vol. 12, p. 219.
4. Tan, S.H. and Kounaves, S.P., *Electroanalysis*, 1998, vol. 10, p. 364.
5. Ferri, T. and Sangiorgio, P., *Anal. Acta*, 1999, vol. 385, p. 377.
6. Badr, Y. and Mahmoud, M.A., *Physica B*, 2005, vol. 369, p. 278.
7. Remigiusz Kowalik and Krzysztof Fitzner, *J. Electroanal. Chem.*, 2009, vol. 633, p. 78.
8. Zein El Abedin, S., Saad, A.Y., Farag, H.K., Borisenko, N., Liu, Q.X., and Endres, F., *Electrochim. Acta*, 2007, vol. 52, p. 2746.
9. Yanqing Lai, Fandyang Liu, Jie Li, Zhian Zhang, and Yexiang Liu, *J. Electroanal. Chem.*, 2010, vol. 639, p. 187.
10. Kargar Razi, M., Maamoury, R.S., and Banihashemi, S., *Int. J. Nano. Dim.*, 2011, vol. 1, P. 261.
11. Gurin, V.S., Prokopenko, V.B., Alexeenko, A.A., Wang, Sh., and Prokoshin, P.V., *J. Mater. Sci. Eng. C*, 2001, vol. 15, p. 93.
12. Haiqing Jiang, Xi Yao, Jun Che, Minqiang Wang, and Fantao Kong, *J. Ceram. Int.*, 2004, vol. 30, p. 1685.
13. Wandong Zhang, Yamin Chai, Nana Cao, and Yonglan Wang, *J. Mater. Lett.*, 2014, vol. 134, p. 123.
14. Yuan-tao Chen, Wei Zhang, Yan-qing Fan, Xiao-qing Xu, and Zhong-xin Zhang, *J. Mater. Chem. Phys.*, 2006, vol. 98, p. 191.
15. Zhenghua Wang, Xiangying Chen, Jianwei Liu, Xiaogang Yang, and Yitai Qian, *J. Inorg. Chem. Commun.*, 2003, vol. 6, p. 1329.
16. Martínes-Escobar, D., Ramachandran Manoj, Sánchez-Juárez, A., Naroo Rios, and Jorge Sergio, *J. Thin. Solid Films*, 2013, vol. 535, p. 390.
17. Ubale, A.U. and Sakhare, Y.S., *J. Vacuum*, 2014, vol. 99, p. 124.
18. Xuchuan Jiang, Brian Mayers, Yuliang Wang, Bryan Cattle, and Younan Xia, *J. Chem. Phys. Lett.*, 2004, vol. 385, p. 472.
19. Sheng-Yi Zhang, Juan Zhang, Yi Liu, Xiang Ma, and Hong-Yuan Chen, *Electrochim. Acta*, 2005, vol. 50, p. 4365.
20. Josef Pola, Zdenek Bastl, Jan Subrt, and Akihiko Ouchi, *J. Appl. Surf. Sci.*, 2001, vol. 172, p. 220.
21. Mendoza, D., Lbpez, S., Granandos, S., Morales, F., and Escudero, R., *J. Synth. Metals*, 1997, vol. 89, p. 71.
22. Abdel Aal, A., Voigts, F., Chakarov, D., and Endres, F., *Electrochim. Acta*, 2012, vol. 59, p. 228.
23. Bartosz Maranowski, Marcin Strawski, Wojciech Ososwiecki, and Marek Szklarczyk, *J. Electroanal. Chem.*, 2015, vol. 752, p. 54.
24. Cabral Murilo, F., Suffredini Hugo, B., Pedrosa Valber, A., Tanimotoa Sonia, T., and Machado Sergio, A.S., *J. Appl. Surf. Sci.*, 2008, p. 5612.
25. Steichen, M. and Dale, Ph., *J. Electrochem. Commun.*, 2011, vol. 13, p. 865.
26. Sheng-Yi Zhang, Juan Zhang, Yi Liu, Xiang Ma, and Hong-Yan Chem, *Electrochim. Acta*, 2005, vol. 50, p. 4365.
27. Cattarin, S., Furlanetto, F., and Musiani, M.M., *J. Electroanal. Chem.*, 1996, vol. 415, p. 123.
28. Scharifker, B. and Hills, G., *Electrochim. Acta*, 1983, vol. 28, p. 879.
29. Gunawardena, G., Hills, G., Montenegro, T., and Scharifker, B., *J. Electroanal. Chem.*, 1982, vol. 138, p. 225.
30. Santos Mauro, C. and Machado Sergio, A.S., *J. Electroanal. Chem.*, 2004, vol. 567, p. 203.
31. Cavallini, M., Aloisi, G., and Guidelli, R., *Langmuir*, 1999, vol. 15, p. 2993.
32. Senthikumar, M., Mathiyarasu, J., Joseph James, Phani, K.L.N., and Yegnaraman, V., *Mater. Chem. Phys.*, 2003, vol. 108, p. 403.
33. Cerisier, M., Attenborough, K., Celis, J.P., and Van Haesendonck, C., *Appl. Surf. Sci.*, 2000, vol. 166, p. 154.
34. Gomez, E., Pollina, R., and Vallés, E., *J. Electroanal. Chem.*, 1997, vol. 397, p. 111.
35. Sauthampton Electrochemistry Group, in *Instrumental Methods in Electrochemistry*, Kemp, T.J., Ed., Ellis UK, Horwood Ltd., Chichester, 1985.
36. Grujicic, D. and Pesie, B., *Electrochim. Acta*, 2004, vol. 29, p. 4719.
37. Floate, S., Hyde, M., and Compton, R.G., *J. Electroanal. Chem.*, 2002, vol. 523, p. 49.
38. Budevski, E., Staikov, G., and Lorenz, W.J., *Electrochemical Phase Formation and Growth*, Weinheim: VCH, 1996.
39. Volmer, M., *Kinetics of Phase Formation*, Dresde: Steinkopff, 1939.
40. Hagfeldt, A. and Grätzel, M., *Chem. Rev.*, 1995, vol. 95, p. 49.
41. Gonzalez-Hernandez, J., Gorley, P.M., Holrley, P.P., Vartsabyuk, O.M., and Vorobiev, Yu.V., *Thin Solid Films*, 2002, vol. 403–404, p. 471.
42. Yamaguchi, T., Yamamoto, Y., Tanaka, T., Tanashi, N., and Yoshida, A., *Sol. En. Mate. Sol. Cells*, 1998, vol. 50, p. 1.
43. Huang, C.J., Meen, T.H., Lai, M.Y., and Chen, W.R., *Sol. En. Mater. Sol. Cells*, 2004, vol. 82, p. 553.
44. Sadigov, M.SW., Ozkan, M., Bacaksiz, E., Altunbas, M., Kopya, A.I., *J. Mater. Sci.*, 1999, vol. 34, p. 4579.
45. Singh, R.P., Singh, S.L., and Chandra, S., *J. Phys. D: Appl. Phys.*, 1986, vol. 19, p. 1299.
46. Pejova, B. and Grozdanov, I., *Appl. Surf. Sci.*, 2001, vol. 1777, p. 152.